Parametric Set-Up of a Structural Model for FERMAT Configuration for Aeroelastic and Loads Analysis

(Received: Jan. 3 2014. Revised: Mar. 14, 2014. Accepted: May 1, 2014)

Thomas Klimmek[1]

Abstract

The development of a structural finite element model for the generic aircraft configuration named FERMAT is presented. The geometry of the FERMAT configuration is based on the NASA Common Research Model (CRM). The CRM is a wing/body/nacelle/pylon/horizontal-tail configuration that was originally developed for the AIAA 4th Drag Prediction Workshop in 2009. It is based on a long-range, wide-body transonic transport. For the FERMAT configuration the geometry and position of a vertical stabilizer is defined as well as missing overall aircraft characteristics. The development of the structural model for the complete aircraft configuration is presented, where a parametric modeling approach is applied and methods from Computer Aided Geometric Design (CAGD) are used. A design process is established, comprising the parametric modeling part, loads analysis, and the sizing of the structure taking consideration of structural and aeroelastic constraints. The parametric approach enables a wide range of variations while the structural model for the wing-like components is as detailed as possible. The parametric design loop has three basic sequential steps. It starts with the set-up of parameterized simulation models (e.g. finite element model, aerodynamic model, mass models, and optimization model) for the given target flight shape. It follows an aeroelastic loads analysis using the condensed structural model for selected mass cases. And finally, the structural components are sized independently using the detailed structural models: for the wing, aileron effectiveness is also defined as a constraint. After adapting the jig shape of the wing, the process is repeated until the structural sizing and the jig-shape converge. The structural dynamic characteristics are presented for two mass cases. The final flutter investigation is briefly described and in doing this an advantage was derived by adopting the parametric approach. In order to avoid the first flutter mode being at the horizontal stabilizer, the structural concept of the load carrying structure of the horizontal stabilizer was modified and the design process repeated.

1 Introduction

Publicly available structural models of generic, but also at the same time realistic and state of the art aircraft configurations to be used for aeroelastic analysis are rare. It is understandable that aircraft manufacturers are reluctant to distribute confidential data about their products or company internal research configurations. But structural models developed in the course of publicly funded research projects are also normally only distributed among the project partners to undertake the task defined for the particular project. As examples, structural models were developed in the course of the project 3AS (2002-2005), funded by the European Commission (EC). In 3AS [23] the EuRAM [13], the X-DIA [21], and the HARW [9] configurations were set-up and corresponding simulation models established for aeroelastic and aero-servoelastic analysis.

The CRM configuration, originally developed for the AIAA 4th Drag Prediction Workshop [25], seems to be a promising configuration also for aeroelastic analysis as far as the wing is optimized for M=0.85. For transonic regime, unsteady aerodynamic phenomena such as shock induced separation effects are expected to cause non-linearities and could influence the flutter boundary. First

[1] Research Scientist, Institute of Aeroelasticity, DLR German Aerospace Center, Göttingen, Germany

doi:10.3293/asdj.2014.27

aeroelastic applications with the CRM configuration have already been performed and documented in [27] and [26]. In the latter the configuration name FERMAT is introduced. The CRM is also appealing, because the size and the overall aircraft parameters are comparable to known long-range wide-body aircraft configurations.

The basic requirements for structural models to be applicable for aeroelastic and loads analysis are the proper modeling of global mass and stiffness characteristics. Regarding the mass model, a variety of mass configurations also have to be set up adequately. A wide range of fuel/payload/passenger conditions are required by the regulations to be considered for loads or flutter analysis.

Furthermore, the stiffness characteristics along the so-called load reference axis (LRA) have to be sufficiently reasonable for aeroelastic analysis. The use of comprehensive structural models representing the structural design in adequate detail allows for the application of state-of-the-art structural optimization methods (e.g. for aeroelastic tailoring) and adopts the trend of using simulation models that are as detailed as possible in early stages of designing an aircraft.

By way of example, the multidisciplinary optimization (MDO) loop developed at the aircraft manufacture Fairchild-Dornier is mentioned [22], where within the MDO loop almost all specialist departments were involved. A design tool to establish structural models for aeroelastic analysis in the conceptual design stage is NeoCASS, developed during the EC-funded project SimSAC [5].

The presented process is established to set up a generic structural model of the FERMAT configuration. The wing-like components are in terms of the size and the level of detail, at a preliminary design level using shell and beam elements. The fuselage and the engine pylon are modeled with beam elements. A condensed structural model defined along the LRA can be derived from the detailed model. The condensed structural model is defined along the LRA. Furthermore various mass configurations can be established. For the FERMAT, the mass configurations C1 and C2 are finally prepared. C1 is a maximum zero fuel weight configuration, while C2 has maximum take-off weight with 100% fuel. The set-up of the mass configuration is also based on the parametric approach.

2 Completion of the FERMAT Configuration

The FERMAT configuration is based on the NASA Common Research Model (CRM) developed for the 4th Drag Prediction Workshop. The CRM is a wing, fuselage and horizontal tail configuration. The geometry of the nacelle is visualized in [25], but is not part of the publicly available IGES geometry. The wing itself is the result of an aerodynamic-structural optimization study [11]. The development of the CRM model, such as the wing/fuselage integration or the design of the horizontal tail is described in [25].

In the following section the missing aircraft parameters are defined and the design of vertical stabilizer is presented. Minor adaptations, like the z-position of the engine and definition of the landing gear positions are described as well. The fully defined aircraft configuration FERMAT is displayed in Figure 1.

The z-position of the engine as depicted from a picture in [25] is slightly moved upwards, otherwise the landing gear height would be unrealistic. The geometry of the nacelle was primarily designed to ease the CFD grid generation [25] of the configuration with nacelle. The main landing gear (MLG) is positioned with sufficient distance behind the defined center of gravity range. The position of the nose landing gear is set to a reasonable position in the front zone of the fuselage.

2.1 Design Weight Characteristics

In order to define the design weights, the FERMAT is compared to known aircraft of similar size. The basic geometrical data for the FERMAT is listed in

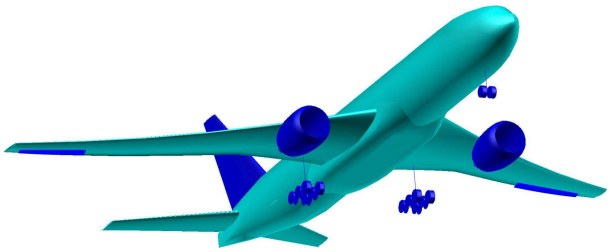

Figure 1: Geometry FERMAT configuration with CRM parts and new components.

Item	CRM
Wing Area [m^2]	383.7
Span [m]	58.0
Reference Chord [m]	7.005
Leading Edge Wing Sweep [°]	35.0
Fuselage Length [m]	62.75
Fuselage Diameter [m]	6.2

Table 1: Basic geometrical parameter of the CRM respectively FERMAT configuration.

Table 1. Therefore the maximum take-off weight (MTOW) is set to 260000 kg and the maximum zero fuel weight (MZFW) to 195000 kg The operation weight empty (OWE) is set to 134000 kg as a result of a group weight assessment using conceptual designing formula from [20].

The center of gravity range is defined between 32.947 m and 34.759 m from origin or 14%-40% mean aerodynamic chord (MAC). The origin is located 2.35 m ahead of the nose.

2.2 Design Speeds and Altitude

The maximum operating limit speeds V_{MO} and M_{MO} are set to 375KEAS and $M_{MO} = 0.92$ in order to keep reasonable distance to the cruise Mach number of M=0.85. Furthermore it is defined that the design cruise speed $V_C = V_{MO}$ and respectively $M_C = M_{MO}$. The design dive speed is set to $V_D = 431$KEAS and $M_D = 0.99$. The value of M_D results from the equation $M_D = M_C + 0.07$ given in AMC 25.335(b)(2) 4b of the CS25 regulations [19]. The design speed V_D is estimated as $V_D = f(V_C)V_C$ using $f(V_C)$ from the worksheet BM 32 100-05 of the "'Luftfahrttechnisches Handbuch"', the German Aeronautical Engineering Handbook [16]. The transition altitude is 7640mfor V_C/M_C and 6524m for V_D/M_D.

2.3 Design of the Vertical Stabilizer

For the FERMAT configuration no vertical stabilizer has been designed yet. In order to keep effort to minimum, basic conceptual design rules were applied and available data of existing aircraft consulted for the design of the geometry and position of the vertical stabilizer. In Table 2 the basic data of the resulting vertical stabilizer is listed and in Figure 2 the dimensioned planform is displayed.

Although the recommended value of 0.09 [20] for the vertical stabilizer volume is higher than the actual value of 0.065, for comparable aircraft found the values for c_{VT} were similar.

2.4 Design of the Aileron Size and Position

Since for the FERMAT configuration no control surfaces for roll are defined, the size and position of the ailerons are estimated using methods from conceptual design. An aileron setting is chosen where an inner and an outer aileron are defined at the outer wing next to high-lift flaps. The inner aileron is used for high speed. Later in the paper, investigations regarding the aileron efficiency are

Table 2: Geometrical data of new vertical stabilizer.

Parameter	Value
Area	58.748 m^2
Height	10.582 m^2
Aspect Ratio	1.911
Taper Ratio	0.273
Root Chord	8.729 m
Tip Chord	2.382 m
Mean Aerodynamic Chord	6.15 m
Leading edge sweep	45.5
Profile thickness	10°
Profile type	NACA0010
Lever arm	24.888 m
Vertical tail volume	0.065

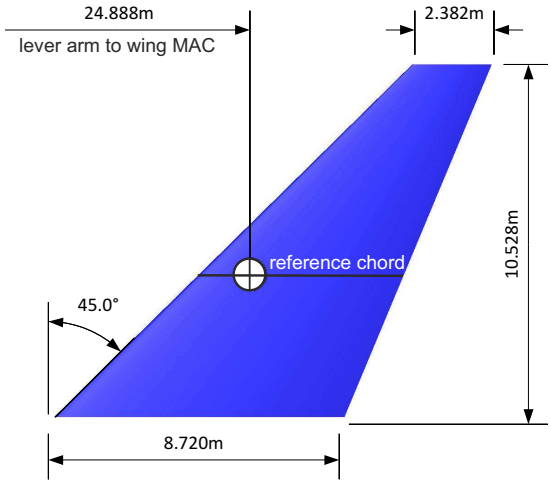

Figure 2: Dimensioned planform of the designed vertical tail.

Table 3: Aileron parameter.

Parameter	Value	Recommended Values [10]
S_A	11.183 m^2	
b_A/b	0.20	0.21
c_A/c	0.25	0.29
y_A/b	0.425	0.42
S_A/S	0.0301	0.032
V_A	0.0124	0.013

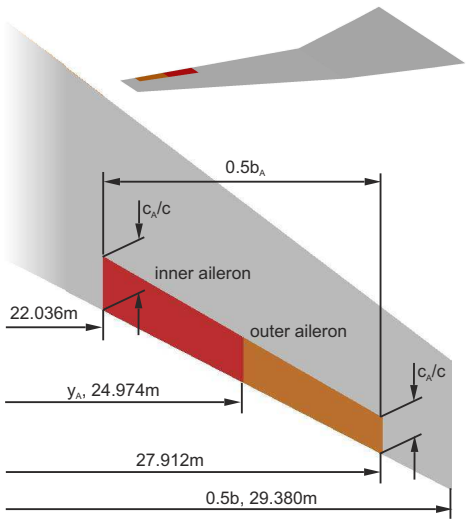

Figure 3: Aileron dimensions.

performed. Therefore only the inner aileron is taken into consideration where only high speed roll performance is considered.

In Figure 3 the dimensions of the inner and outer aileron are displayed. The inner and outer aileron are of the same length. In Table 3 recommended design parameters for the aileron design are given as well as the actual value. Although not all recommended parameter values can be achieved, the aileron volume V_A with $V_A = 0.5 S_A l_a / Sb$, where $l_a = 2y_A$, and selected other parameters are at least close to the recommended values.

3 Parametric Modeling Using CAGD Methods

The set-up of all simulation and optimization models is based on one overall parametric modeling concept using geometric objects and differential geometric methods from Computer Aided Geometric Design (CAGD). For the outer geometry of the wing-like components and nearly all parts of the load carrying structure, B-spline curves and surfaces are applied in order to describe them as geometrical objects. Curves are mainly set up by approximation of points. The points themselves are estimated either by evaluation on parametric surfaces or resulting from curve/plane or curve/surface intersections. Surfaces are normally defined by blending of B-spline curves.

The basic formulation of B-splines is given as follows:

$$\boldsymbol{p}(u) = \sum_{i=0}^{n} \boldsymbol{d}_i B_{i,k}(u). \tag{1}$$

for $n+1$ control points $\boldsymbol{d}_i$. The $B_{i,k}$ are weighing functions of polynomials of the degree $k-1$ and the knot values t_i and t_{i+1}. They are defined as follows:

$$\begin{aligned} B_{i,1}(u) &= 1 \quad \text{for} \quad u \in [t_i, t_{i+1}] \\ B_{i,1}(u) &= 0 \quad \text{for} \quad u \notin [t_i, t_{i+1}] \end{aligned} \tag{2}$$

and the recursive formulation

$$B_{i,k}(u) = \frac{(u - t_i) B_{i,k-1}(u)}{t_{i+k-1} - t_i} + \frac{(t_{i+k} - u) B_{i+1,k-1}(u)}{t_{i+k} - t_{i+1}} \tag{3}$$

Further information regarding CAGD methods or B-spline functions in particular can be found in [15], [7], or [3].

The analytical formulation of curves and surfaces allows also for the evaluation of derivatives or normal vectors to be used in the parametric modeling process. Furthermore, geometry transformation like translation, rotation, and scaling are applied as well as the definition of local coordinate systems.

In Figure 4a for example the B-spline curve $\boldsymbol{r}_1(u_1)$ is used to define the airfoil geometry and the curve $\boldsymbol{r}_2(u_2)$ represents the camber line. The latter is used to generate a surface out of all camber line curves eventually to be used to estimate correction factors for the doublet lattice aerodynamic model. Thus camber and twist can be incorporated.

Figure 4b shows geometrical objects of the right horizontal tail wing. The B-spline surface $\boldsymbol{p}_3(u_3, v_3)$ for example defines the lower outer geometry of the right horizontal tail wing. Furthermore $\boldsymbol{p}_4(u_4, v_4)$ is the B-spline surface for the upper skin surface between two ribs, later in the modeling process to be used to estimate the FEM nodes and elements. The analytical functions for the curves are defined in the interval $u_i \in [0; 1]$ and the surfaces accordingly with $u_i, v_i \in [0; 1] \times [0; 1]$.

The level of detail of the structural model of the wing-like structural models is such that all main structural parts of a wing are modeled with finite elements. This comprises the basic parts such as skin, spars, and ribs as well as stiffener elements such as stringer, spar caps or inner stiffener elements reinforcing spars and ribs.

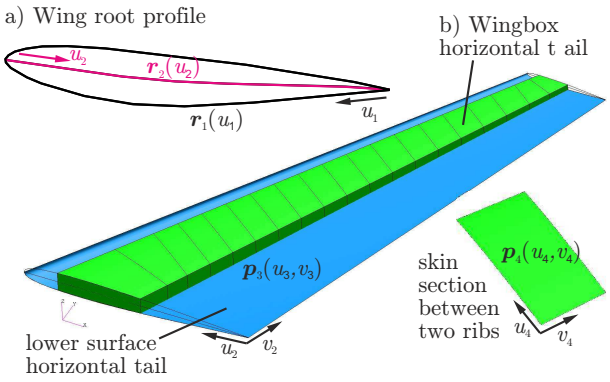

Figure 4: Analytical geometrical functions of a) wing profile and b) horizontal tail outer geometry and geometry of the load carrying structure.

4 MONA: Modeling, Loads, and Sizing Loop

The process to set up the structural model of the FERMAT configuration is carried out with a loop, as it is shown in Figure 5. Basically the process starts with the set-up of all simulation and optimization models in terms of components. The loop is called MONA, because the main acting programs are the DLR program ModGen, setting up all kinds of simulation models, and the program MSC Nastran.

4.1 Model Set-up

A brief overview of all disciplinary simulation models involved is given in Figures 6a-n. They are created in the course of a step-by-step modeling process and assembled into a detailed finite element model for the complete aircraft as is displayed in Figure 6o. The condensed structural model (see Figure 7) is then derived from the detailed model. For the set-up of the simulation models the DLR-AE internal computer program ModGen is used, where parametric modeling techniques based on CAGD are applied as described in Section 3.

4.2 Detailed Finite Element Model

The detailed and the condensed structural models consist of a massless stiffness model and a mass model. The mass items are attached to the structure at the nodes of the load reference axis. This modeling technique allows for a smooth application of various mass models to the same stiffness model. Furthermore the local modes are avoided

The detailed finite element model has 23859 nodes, 58254 shell and bar elements, and 143094 degrees of freedom (DOFs). Stringer, spar caps, and inner stiffener of spars and ribs are modeled with beam elements (see Figure 6g). The distributed stiffener elements keep the buckling fields to a reasonable size. The stringers run parallel to the front spar. The load carrying structures of the horizontal and the vertical tailplane are modeled similarly. The fuselage model consists of beam elements, representing the global stiffness properties of a circular cross section (see also Figure 6f).

4.2.1 Mass Model

The mass items are attached at the nodes of the load reference axis and the engine position respectively. The detailed finite element model contains mass items as follows:

- structural mass section, based on sections of the load carrying structure of wings and tail from shell/beam models (see Figure 8),
- across-the-board estimation of additional mass for leading and trailing edge of the wing and the tail. For the set-up of distributed mass items

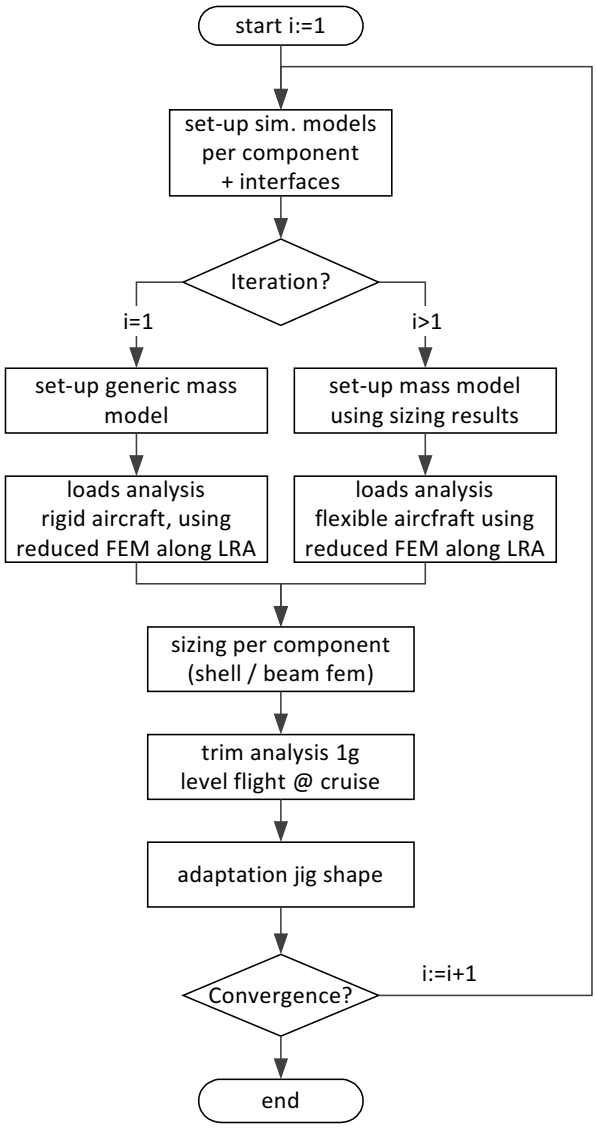

Figure 5: MONA, the model set-up, loads analysis, and sizing loop.

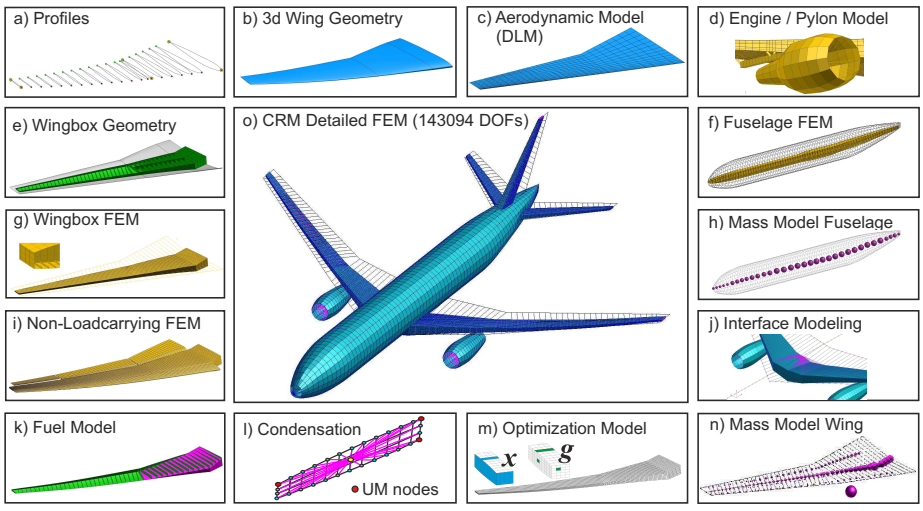

Figure 6: Simulation and optimization models of FERMAT configuration.

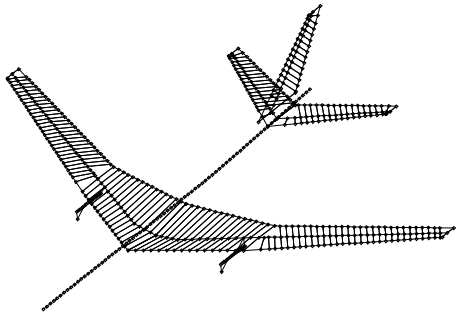

Figure 7: Condensed finite element model of the FERMAT configuration.

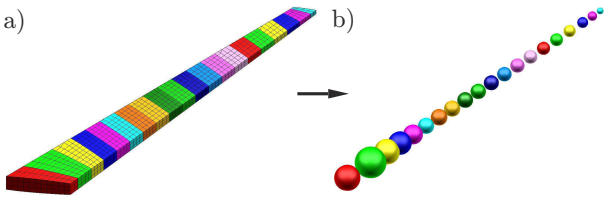

Figure 8: a) FEM of right horizontal tail wing box with colored rib center bays, b) mass item per rib center bays

shell models only for mass modeling are created according to the estimated mass values according to [24], see Figure 6i and 6n,

- across-the-board estimation of additional mass for the wing due to sheet taper and joints in skin-stringer panels and large cut-outs according to [24], see Figure 6i and 6n,
- estimation of the mass for the engine and the pylon according to [20],
- estimation of the mass of the nose and main landing gear according to [20],
- estimation of section wise structural mass of the load carrying structure of the fuselage according to [2],
- distributed mass items attached to the fuselage load reference axis nodes representing the system mass, defined payload/passenger mass, and fuel mass.

The parameterization concept allows for the set-up of specific fuel mass models considering specified filling levels per tank and a defined deck angle of the aircraft. Out of the intersection of a plane, representing the surface of the fuel, with the surfaces of two ribs in succession (fuel bay) one volume element is defined (see Figure 6k). Finally the mass properties of all volume elements per fuel bay (mass and inertia) and the center of gravity are estimated. Also considered is that, for integral tanks 85% of the measured volume is usable [20]. Similar to other aircraft, three tanks are defined for the FERMAT configuration: a center tank located within the center wing box (ribs 1-5), an inner tank from rib 5 to rib 35 and an outer tank from rib 35 to rib 47, the tip of the wing box (see also Figure 9).

Three different fuel mass models are considered in the course of MONA. The fuel model 016 has 70% fuel and is used for the load cases where the aircraft is at MTOW. Fuel model 014 is used for optimization step 3, where only aileron effectiveness is defined as a constraint. This fuel model is also taken for the 1g

Table 4: FERMAT fuel mass per fuel tank of the right wing.

fuel	tank volume [liter]				
code	center	inner	outer	total	[%]
004	20880	42194	2654	65728	100%
014	20880	12799	0	33769	51.4%
016	20880	25412	0	46292	70.4%

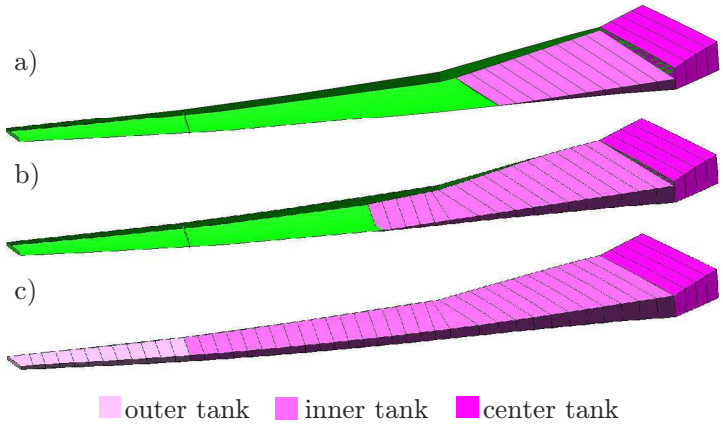

Figure 9: Three fuel models, a) f014 with 51.2% filling, b) f016 with 70.4%, and c) f004 with 100%.

trim analysis that is done to estimate the jig shape. Finally the fuel model 004 has 100% filled fuel tanks. It belongs to the C2 configuration of the available finite element model. C2 is also an MTOW configuration. In Table 4 the volumes of each tank are listed for all considered fuel models.

4.3 Condensed Finite Element Model

The condensed structural model has in total 276 nodes. They are defined on the LRA of the wing, tail, fuselage, the pylon, and at the engine center of gravity position. For the wing-like components, additional nodes are defined at the leading and trailing edge with rigid connection to the corresponding node on the LRA.

The LRA nodes are placed in the ribs plane and connected to the border grids of the ribs with the interpolation element RBE3 of MSC Nastran. Though the RBE3 element is not a rigid body element and is not stiffening the structure, the DOFs of the LRA node are treated like multipoint constraints and are therefore put into the so-called m-set of the stiffness matrix. The m-set, containing all multipoint constraint DOFs, is a subset of the so-called g-set stiffness matrix, which contains all DOFs of all nodes. Nodes in the m-set can not be used for the condensation. Therefore the condensation of the stiffness to the load reference axis of the wing-like components is done by using the UM option of the RBE3 element. Three nodes from the border of the ribs, forming a triangle, are selected and six DOFs of the three nodes are reassigned to the m-set instead of the six DOFs of the LRA node. (see also Figure 6l). The UM nodes and the DOFs are chosen to determine the six rigid body motions of the RBE3 element. The static condensation is finally done by assigning the LRA nodes to the so-called a-set of the finite element model.

Two mass configurations C1 and C2 are defined. The first, C1, has a mass of 195000 kg, the maximum zero fuel weight (MZFW), with 25194 kg representing the passenger load and 30260 kg for the payload. C2 is an MTOW configuration with a mass of 260000 kg. According to fuel model 004 the fuel tanks are 100% filled. The center of gravity position for both is located at 25% MAC or x=33.714 m from the origin. The origin is 2.35 m ahead the fuselage. The mass entities are linked to the LRA nodes, while the shell and beam elements of wing-like components are massless.

4.4 Loads Analysis

The loads are estimated by a static aeroelastic trim analysis of the complete aircraft. The basic equation is defined as follows:

$$(\boldsymbol{K}_{aa} - q\boldsymbol{Q}_{aa})u_a + \boldsymbol{M}_{aa}\ddot{u}_a = q\boldsymbol{Q}_{ax} + \boldsymbol{P}_a \tag{4}$$

with the structural stiffness matrix $\boldsymbol{K}_{aa}$, the aerodynamic influence coefficient matrix $\boldsymbol{Q}_{aa}$ the structural mass matrix $\boldsymbol{M}_{aa}$, the matrix $\boldsymbol{Q}_{ax}$ providing the forces at the structural grid points due to deflection of aerodynamic extra points (e.g. aileron), the vector of applied loads $\boldsymbol{P}_a$, and the dynamic pressure q . The matrices are defined in the so-called a-set, where only the nodes of the LRA, the pylon and at the engine are considered.

The resulting force and moments acting on the a-set nodes are the aerodynamic and inertia loads with $P_a^{aero} = q\boldsymbol{Q}_{aa}u_a$ and $P_a^{inertia} = \boldsymbol{M}_{aa}\ddot{u}_a$ respectively. In iteration 1, the structure is considered as rigid and from iteration 2 onward the structural flexibility is taken into account. In total, 10 load cases are considered.

The load cases 1 to 8 are symmetric pull-up maneuver with $n_z = 2.5g$ defined for two mass configurations (MTOW and MZFW) with front center of gravity position and four flight conditions (V_C and V_D at sea level and transition altitude). For the MTOW mass configuration 70% fuel is considered (fuel model 016). It is noted that MTOW can also be reached with partially filled fuel tanks. An example for an MTOW configuration with 100% fuel is the C2 configuration. The remaining two load cases are yawing maneuver with positive and negative rudder deflection of 15° for V_C at transition altitude and MTOW as mass configuration.

For the loads acting on the vertical tail two antisymmetric quasi static yaw maneuvers are performed for mass configuration MZFW with front center of gravity position and one flight condition (load cases 9 and 10, V_C at sea level with $\beta = +5$ and $\beta = -5$ rudder angle). It is noted that such roughly defined load cases are only a starting point for the loads analysis with respect to the vertical tail.

4.5 Structural Sizing

The structural sizing of the wing is done in three steps. In the first step the structural properties, such as skin, spar, rib thickness and the cross-section area of stringer and spar caps are based on cutting loads. For the 2nd and 3rd steps mathematical optimization algorithms are applied, using MSC Nastran SOL200 [1].

The structure is sized component-wise using different approaches for the wing, the tailplane, and the fuselage.

Wing

For the wings a three-step approach is used. In the first step, the wing box shell and beam elements are sized according to [6] at defined cross-sections with the cutting shear force $\boldsymbol{F}_z$, wing bending moment $\boldsymbol{M}_x$, and torsion moment $\boldsymbol{M}_y$. This procedure is also called preliminary cross section sizing (PCS). The cross sections of the wing box are approximated by a rectangles having mean width and height compared to the actual cross-sections. The upper and lower skin field between two consecutive ribs are dimensioned with $\boldsymbol{M}_x$.

Local buckling at the skins is taken into account due to the consideration of simultaneous skin and stringer buckling [8]. The stringer dimensions (e.g. for Z-stringer) are estimated for a given stringer pitch and the amount of material that is available for the stringer. The amount of material to be used for spar caps translated to dimensions of T-shape spar caps. Spars are sized with $\boldsymbol{F}_z$ and $\boldsymbol{M}_y$. The ribs are sized according to the dimensions of spars next to a rib. Furthermore, allowable stress values for buckling are estimated. The dimensions of the inner stiffener of the spars and ribs depend on the thickness of the corresponding rib and spar zone.

In total, the thickness and in each case the beam dimensions are estimated with PCS for 328 design fields (see Table 5).

Component	Nb DV	
	PCS	SOL200
Upper skin center wing box	4	8
Lower skin center wing box	4	8
Upper skin wing box	42	418
Lower skin wing box	42	418
Stringer	92	0
Spar	46	107
Spar caps	46	0
Ribs	52	52
Total	328	1011

Table 5: Design variables for the various sizing steps.

Constraint Type	SOL200 Sizing	
	Step 2	Step 3
Von Mises stress	70496	0
Compression buckling (skins)	31792	0
Shear buckling (spars, ribs)	38704	0
Aileron effectiveness	0	1
Total	140992	1

Table 6: Design constraints for MSC Nastran optimization.

In the second step, gradient-based sizing optimization is done using mathematical optimization algorithms. The optimization problem is formulated mathematically as follows:

$$Min\{f(\boldsymbol{x})|\boldsymbol{g}(\boldsymbol{x}) \leq 0; \boldsymbol{x}_l \leq \boldsymbol{x} \leq \boldsymbol{x}_u\} \tag{5}$$

with f as the objective function, $\boldsymbol{x}$ as the vector of n design variables, $\boldsymbol{h}$ as the vector of m_h equality constraints, $\boldsymbol{g}$ as the vector of m_g inequality constraints and $\mathbb{R}^n$, the n-dimensional, EUCLIDean space. The definition of the objective function f, the design variables $\boldsymbol{x}$, and the constraints $\boldsymbol{g}$ is called design model. As objective function f the mass of the wing box is defined. The design variables are thicknesses of the skin fields bordered by two consecutive ribs and two stringer. For the spars, the skin between two ribs is treated as one variable, and for the ribs the thickness of a complete rib is defined as one variable.

The constraints are allowable maximum von-Mises stress values for each shell element, and buckling safety factor for each element. For the calculation of the buckling safety factor the allowable buckling stress is calculated with a simplified analytical formula [4]. Compression buckling is considered for the skins, while shear buckling is considered for the spars and ribs. Ten load cases are considered for the sizing. Table 5 shows the design variables for all the sizing steps

The third step takes the results of the design variables from the second step and uses them as lower gage constraint. The objective function is again the wing mass, but the only constraint is a required C_{l,δ_a}. Normally aileron effectiveness is defined as $-C_{l,\delta_a}/C_{l,p}$, the rolling helix angle. According to the regulations the aileron effectiveness has to be greater or equal to zero within the flutter clearance or aeroelastic stability envelope. Because C_{l,δ_a} turns negative in case of aileron reversal, only C_{l,δ_a} can be used as criterion for aileron effectiveness in the third sizing step.

Since the applied Doublet Lattice Method (DLM) is not valid in transonic flight regime and the stability envelope reaches $M = 1.0$, three 1g cruise trim cases for the Mach numbers 0.75, 0.80, and 0.85, and the altitude of the knee of the stability envelope are selected (see Figure 10a). The roll derivatives C_1, C_2, and C_3 are estimated and approximated with 2nd order polynomial $f(Ma)$. Then f is transposed to $f^\star$ for which C_{l,δ_a} is zero at the knee of the aeroelastic stability envelope (see C_t in Figure 10b). Therein the maximum true airspeed and dynamic pressure occur respectively. For one of the three Mach numbers,

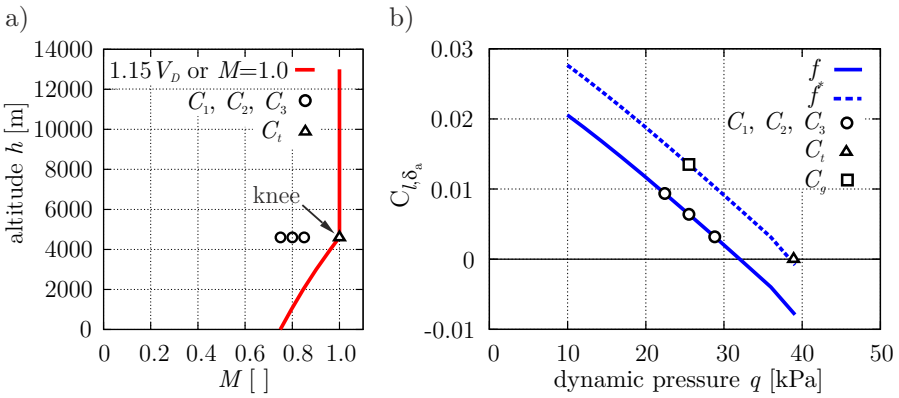

Figure 10: a) Aeroelastic stability envelope, b) Approximation of f with $f^\star$ over dynamic pressure q.

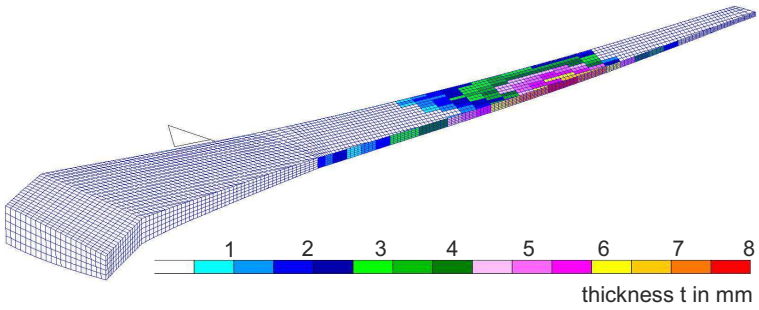

Figure 11: Typical thickness increase for a sizing optimization with aileron effectiveness as the only constraint.

e.g. $M = 0.80$, the value for C_{l,δ_a} is estimated with $f^\star$. Such value of C_{l,δ_a} (C_g in Figure 10b) is used as lower boundary in the sizing step 3, where C_{l,δ_a} is defined as constraint.

It worths stressing that the three selected Mach numbers fall in the transonic regime. Therefore the accuracy of the results from uncorrected DLM may be questionable. This can be solved in future works aiming at including correction to DLM matrices for critical flight points

A typical result of an optimization with respect to the element thickness where only aileron effectiveness is defined as constraint and loads-based optimized dimensions are taken as lower bound is shown in Figure 11.

HTP and VTP

The horizontal and vertical tail are sized in the same way as the wing, excluding step 3 insofar control surface efficiencies are not taken into account.

Fuselage

Since the fuselage is modeled with beam elements, the sizing task is to estimate the beam cross-section properties. The sizing procedure is based on [2], where cutting loads are used to estimate the structural properties. Buckling and various construction types such as frame distance or stringer type are considered on a rough scale. The estimated smeared thickness of the circular fuselage shell (skin plus stiffener) and the section diameter are used to estimate the beam properties.

Pylon

The pylon is modeled with beam elements. The dimensions of the pylon beam, carried out as square tube, are chosen in order to achieve modes and frequencies similar to characteristics of known generic aircraft configuration such as the EuRAM [14] (see also Figure 6d).

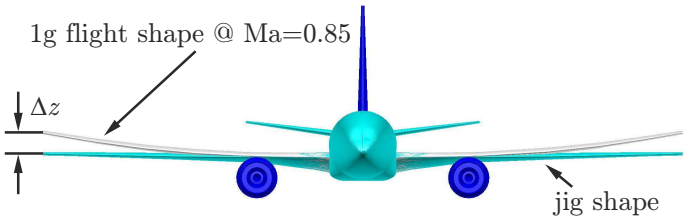

Figure 12: Front-view FERMAT configuration for 1g flight shape at Ma=0.85 and final jig shape.

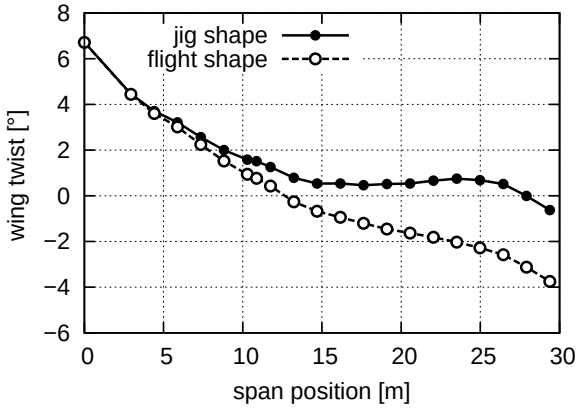

Figure 13: FERMAT twist distribution for flight and jig shape.

4.6 Jig Shape Estimation

The CRM wing geometry is available as a flight shape optimized for a cruise Mach number $M = 0.85$ and and a nominal lift condition of $C_l = 0.5$. Since the loads are estimated from iteration 2 onwards with the flexible structure, it is necessary to apply the loads to the jig shape of the wing. To achieve this, the MONA process is looped. After the sizing of the structure, a trim analysis is performed for 1g level flight at $M = 0.85$ at 35000 ft for a medium mass configuration at a medium center of gravity position (28%MAC). The deflections of the structure are mapped to the leading and trailing edge points of the profile sections that define the geometry of the wing. An alignment of the z-coordinates of the leading and trailing edge points is performed as follows (see also Figure 6a):

$$z_{jig}^{i+1} = z_{jig}^{i} - (z_{flight}^{i} - z_{flight}^{orig}) \tag{6}$$

with z_{jig}^{i} and z_{jig}^{i+1} are the jig shape z-coordinates of iteration i and $i+1$, z_{flight}^{orig} the z-coordinates of the original geometry, and z_{flight}^{i} the resulting z-coordinates of the 1g trim analysis for M=0.85 at 35000 ft for iteration i.

The absolute values of the alignment of the $z-$coordinate and total wing weight after each iteration are used as convergence criteria of MONA. In Figure 12 the flight and the converged jig shape are displayed. It can be noticed that the resulting jig shape of the wing shows almost no dihedral (see Figure 12).

Furthermore, in Figure 13 the initial twist distribution is shown, optimized for the 1g level flight at M=0.85 and $C_l = 0.5$, as well as the resulting twist distribution representing the jig shape of the wing.

5 Results

5.1 Mass Data

In Table 7 the values of the total component mass for the wing, the tail, and the fuselage are compared with the mass values estimated according to literature. Generally the values are in good accordance with the estimated numbers. As the sizing of the wing is based only on eight load cases (symmetric pull-up maneuvers), it is expected that the wing weight would increase in case more

Table 7: Mass breakdown; comparison of values estimated with MONA with non-MONA estimated values.

Component	Mass [kg]	
	MONA	**Estimated**
Wing	31089	33144 [17]
Fuselage	27536	25157 [20]
HTP	2641	2267 [12]
VTP	2231	1564 [12]
Nose Landing Gear	-	1560 [20]
Main Landing Gear	-	9620 [20]
Engine/Pylon	-	19459 [12]
Systems	-	44200 [20]

Table 8: Optimization results for step 1-3.

Sizing Steps	Wing Box [kg]	Δ Mass [kg]
PCS	11040	-
SOL200 stress, buckling constraints	11134	+94
SOL200 aileron effect. constraint	11494	+360

load cases are considered in the sizing process, such as gust loads or landing, and ground loads.

The same is valid for the horizontal tail plane and the vertical stabilizer. Another reason for inaccuracy is the estimation of the masses for the leading and trailing edge parts based on statistics. This method is straight forward and allows also for modeling leading and trailing edges mass items at reasonable positions and with realistic inertia values. A more sophisticated approach would require a detailed investigation regarding loads and modeling itself of such parts.

The overall MONA loop itself shows good convergence as well with the structural sizing step 2 and step 3, where mathematical optimization algorithms are applied. Table 8 shows that the weight increases slightly from step 1 to step 2, although a significant redistribution of the material and concentration to some areas due to more design variables at the skins can be noted (see 14). The consideration of the aileron effectiveness constraints requires another 360 kg of additional material in order to increase the torsional stiffness near the inner aileron. The affected area where the skins and spars are reinforced is shown in Figure 11.

5.2 Static and Dynamic Characteristics

The stress distribution displayed in Figure 15 shows that the maximum allowable von Mises Stress of 256 MPa, is exploited widely at the upper skin. The maximum displacement of 4.53 m occurs at the rear spar of the wing tip, as it can be expected for backward swept wings.

In Table 9 the frequencies of the first ten elastic modes are listed. In Table 10 in addition to the first ten elastic modes, the modes 30 and 31 are listed. Mode 1-6 are rigid body modes. The mass of the completely filled fuel tanks for C2 led to a decrease of the 1st symmetric wing bending from 1.7001 Hz to 1.0574 Hz.

5.3 Flutter Characteristics

For the C1 and C2 configurations a flutter analysis was performed with ZAERO [18]. No flutter mode was found within the flutter clearance envelope. The first two flutter modes appeared at the horizontal stabilizer. The load carrying structure of the horizontal stabilizer was modified to get the first flutter modes at the wing. The modifications comprise an increased sweep of the rear spar

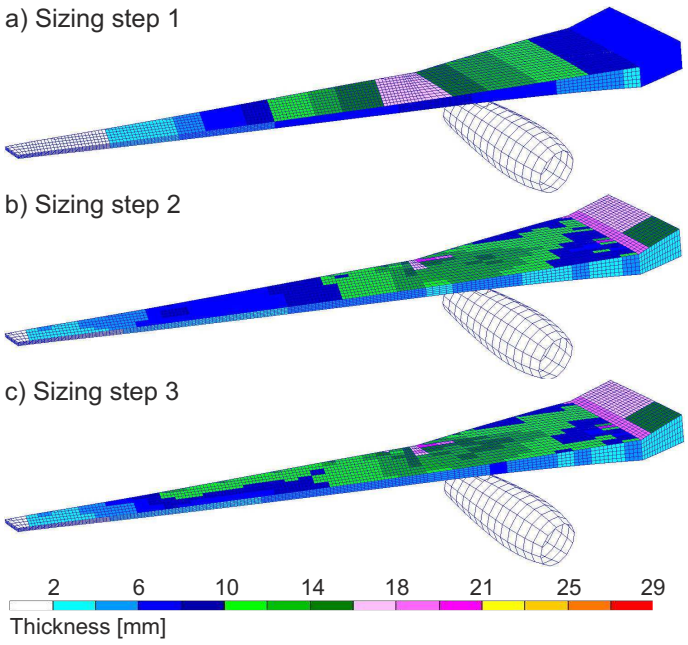

Figure 14: Thickness distribution of the right wing after each sizing step.

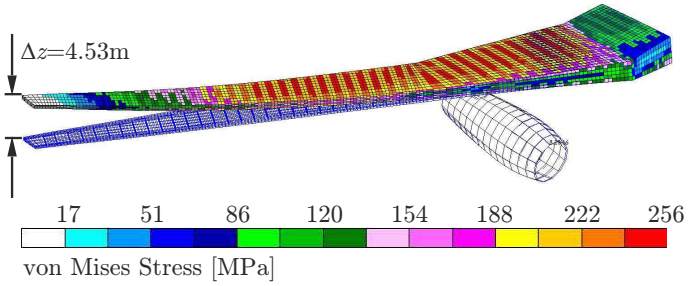

Figure 15: Von Mises stress after sizing optimization with stress and buckling constraint for load case 1 (m=260000kg, nz=2.5g, M=0.57, 375 KEAS).

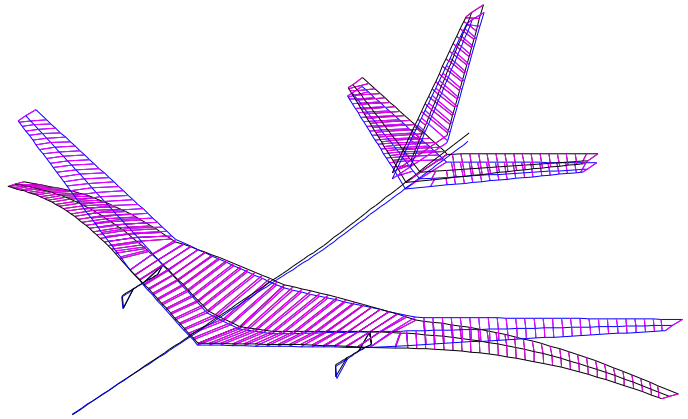

Figure 16: First elastic mode of FERMAT finite element model of C2 configuration @ 1.05Hz.

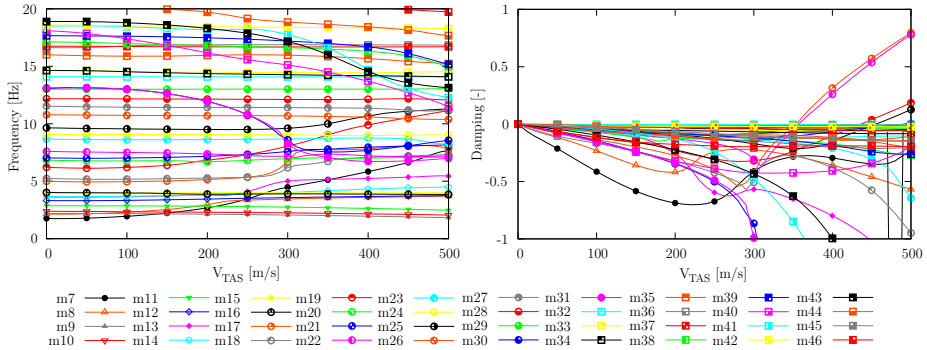

Figure 17: Flutter plots frequency and damping versus velocity for C1 for Ma=0.75 @ sea level

Table 9: Selected elastic modes and frequencies for the configuration C1.

Mode ID	Freq. [Hz]	Mode Description
1-6	≈ 0.0	rigid body modes
7	1.7645	1n symmetric wing bending
8	2.1472	1n antisymmetric wing bending
9	2.2046	symmetric engine pylon lateral bending and roll
10	2.3875	antisymmetric engine pylon roll
11	2.8718	fuselage vertical bending
12	3.3149	fuselage lateral bending
13	3.6353	antisymmetric wing bending
14	3.6719	2n symmetric wing bending
15	3.9778	symmetric wing fore/aft
16	4.0189	antisymmetric wing fore/aft
17	4.9995	3n symmetric wing bending
...		
30	13.0739	symmetric wing torsion
31	13.1211	antisymmetric wing torsion

Table 10: Selected elastic modes and frequencies for the configuration C2.

Mode ID	Freq. [Hz]	Mode Description
1-6	≈ 0.0	rigid body modes
7	1.0574	1n symmetric wing bending
8	1.4547	1n antisymmetric wing bending
9	2.1607	symmetric engine pylon roll + lateral bending
10	2.2924	antisymmetric engine pylon roll + lateral bending
11	2.3917	symmetric wing fore/aft
12	2.4439	antisymmetric wing fore/aft
13	2.7993	fuselage vertical bending
14	2.9894	antisymmetric engine pylon pitch
15	3.0026	fuselage vertical bending
16	3.3693	fuselage lateral bending
...		
30	10.6024	symmetric wing torsion
31	11.1231	antisymmetric wing torsion

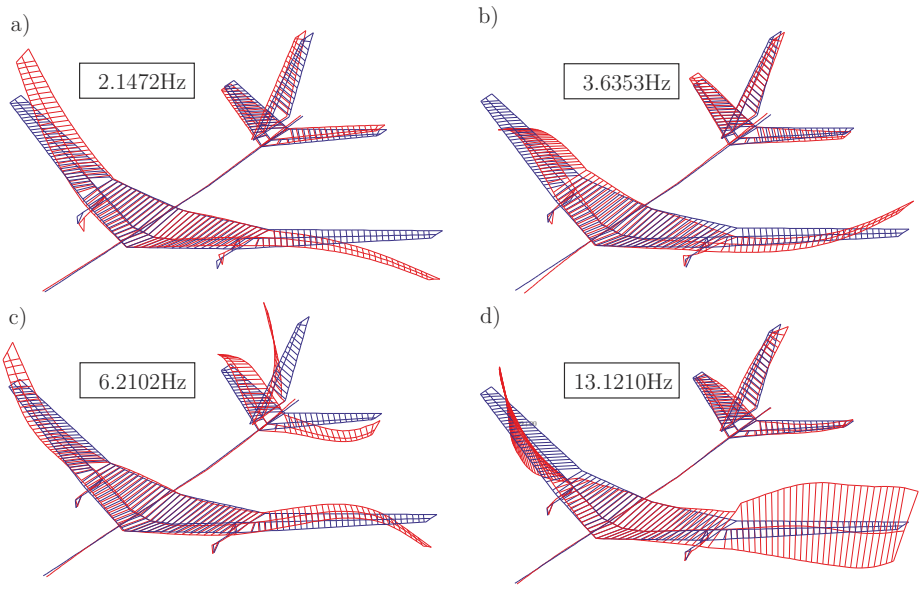

Figure 18: a) to d) Four mode shapes contributing to 1st flutter at 353.4 m/s of C1.

and an additional stringer resulting in an increase of the torsional stiffness. The measures taken resulted in a shift of the horizontal stabilizer flutter modes to far higher speeds.

After the design modifications, the flutter modes with at the lowest speed appear at the wing. The first instability for C1 occurs at 353.4 m/s for the wing. There is a coupling of the antisymmetric modes 8, 13, 19, and 31. Mode 8 is the first antisymmetric wing bending, mode 13 the 2nd antisymmetric wing bending and mode 19 the third antisymmetric bending, wile mode 31 is the first antisymmetric wing torsion. The flutter plots, damping and frequency versus velocity are given in Figure 17 and the four contributing mode shape in Figure 18. The second instability for the wing is observed at 359.9 m/s where the symmetric modes 7, 17, and 30 are coupled. Herein mode 7 is the 1st symmetric wing bending, mode 17 is the 2nd symmetric wing bending, and mode 30 is the 1st symmetric wing torsion.

Since no correction of the subsonic aerodynamic method was carried out, a more thorough investigation using high-fidelity CFD analysis is recommended for a sound assessment of the flutter characteristics of the FERMAT configuration.

6 Conclusions

The set-up of the finite element model for the FERMAT configuration is to be used as a test case for assessment of flutter computation processes adopting CFD and ROMs. The structural model is set up as a detailed structural model where the stiffness and the mass is condensed into load reference axis. The latter is applicable for flutter and loads application. The detailed structural model can be used for sophisticated sizing methods that include the consideration of static aeroelastic constraints such as aileron effectiveness.

By defining the geometry of the vertical tail, the aileron size and position, the landing gear and engine position, and the definition of design mass and design speed values, the definition of the configuration was completed.

A parametric modeling approach was successfully applied in line with a loads and sizing process, the so-called MONA process respectively loop. Design load cases for the sizing of the structure were defined and loads estimated accordingly. The three-step sizing concept showed good convergence and reasonable sizing results especially in terms of the estimated structural component weight.

The consideration of aileron effectiveness as a constraint for the sizing of the wing and the final flutter investigation followed by design modifications for the horizontal stabilizer demonstrates the applicability of the parametric approach to set up structural models for aeroelastic analysis and aeroelastic optimization.

The parametric approach allows for various future parameter studies ranging from definition of the structural concept of wing-like components, the application of different optimization models, the consideration of Carbon Fibre Reinforced Plastic (CFRP) material in line with aeroelastic tailoring methods, or use of high-fidelity aerodynamics for loads and aeroelastic analysis.

References

[1] *MD/MSC Nastran 2010 - Quick Reference Guide*. MSC.Software Corporation, 2010.

[2] M. D. Ardema, M. C. Chambers, A. P. Patron, A. S. Hahn, H. Miura, and M. D. Moore. Analytical fuselage and wing weight estimation of transport aircraft. Technical Report Technical Memorandum 110392, NASA, May 1996.

[3] W. Böhm, G. Farin, and J. Kahmann. A survey of curve and surface methods in CAGD. *Computer Aided Geometric Design*, (1):1–60, 1984.

[4] E. Bruhn. *Analysis and Design of Flight Vehicle Structures*. Tri-State Offset Company, (USA), 1973.

[5] L. Cavagna, S. Ricci, and L. Riccobene. Structural sizing, aeroelastic analysis, and optimization in aircraft conceptual design. *Journal of Aircraft*, 48(6):1840–1855, Nov.–Dec. 2011.

[6] F. V. Dalen. MDO load analysis and preliminary sizing, December 1996.

[7] G. E. Farin. *Curves and Surfaces for Computer Aided Geometric Design*. Academic Press, 1993.

[8] D. J. Farrar. The design of compression structures for minimum weight. *Journal of the Royal Aeronautical Society*, November 1949.

[9] S. Heinze. *Aeroelastic Concepts for Flexible Wing Structures*. PhD thesis, KTH, Royal Institute of Technology, 2005.

[10] D. Howe. *Aircraft Conceptual Design Synthesis*. Number ISBN-10: 1860583016, ISBN-13: 978-1860583018. John Wiley & Sons, 2000.

[11] A. Jameson, J. C. Vassberg, and S. Shankaran. Aerodynamic structural design studies of low-sweep transonic wings. *Journal of Aircraft*, 47(2):505–514, March–April 2010.

[12] I. Kroo. Aircraft design: Synthesis and analysis. Internet, 2012. Course Notes.

[13] S. Kuzmina, F. Ishmuratov, M. Zichenkov, and V. Chedrik. Integrated numerical and experimental investigations of the active/passive aeroelastic concepts on the european research aeroelastic model euram. *ASD Journal*, 2(2):31—51, 2011.

[14] S. I. Kuzmina, V. V. Chedrik, and F. Z. Ishmuratov. Strength and aeroelastic structural optimization of aircraft lifting surfaces using two-level approach. In *6th World Congress of Structural and Multidisciplinary Optimization*, Rio de Janeiro (Brazil), 30 May - 3 June 2005.

[15] M. Mortenson. *Geometric Modeling*. John Wiley and Sons, New York, Chichester, Brisbane, Toronto, Singapore, 1985. ISBN: 0-471-88279-8.

[16] N.N. LTH, Luftfahrttechnisches Handbuch, Ausgabe 2006, 2006.

[17] N.N. *Luftfahrttechnisches Handbuch*. 2006.

[18] N.N. ZAERO User's Manual. ZONA Technology, Inc, 2009. Version 8.3.

[19] N.N. *CS25 - Certification Specifications and Acceptable Means of Compliance for Large Aeroplanes*. http://www.easa.eu.int/home/index.html, 2011. Amendment 11.

[20] D. Raymer. *Aircraft Design: A Conceptual Approach*. AIAA Education Series, Washington, DC, 1989. ISBN 0-930403-51-7.

[21] S. Ricci, A. Scotti, J. Cecrdle, and J. Malecek. Active control of three-surface aeroelastic model. *Journal of Aircraft*, 45(3):1002–1013, May–June 2008.

[22] G. Schuhmacher, I. Murra, L. Wang, A. Laxander, O. J. O'Leary, and M. Herold. Multidisciplinary design optimization of a regional aircraft wing box. In *Proc. of 9th AIAA/ISSMO Symposium on Multidisciplinary Analysis and Optimization*, Atlanta (GA), Sep. 4-6 2002. AIAA.

[23] J. Schweiger, A. Suleman, S. Kuzmina, and Chedrik. MDO concepts for a European research project on active aeroelastic aircraft. In *9th AIAA/ISSMO Multidisciplinary Analysis and Optimization Conference, 4–6 Sept. 2002, Atlanta (GA), USA*, 2002.

[24] E. Torenbeek. Development and application of a comprehensive, design-sensitive weight prediction method for wing structures of transport category aircraft. Report LR-693, TU-Delft, Delft University of Technology, September 1992.

[25] J. C. Vassberg, M. A. DeHaan, S. M. Rivers, and R. A. Wahls. Development of a common research model for applied CFD validation studies, 2008. DPW4 website: http://aaac.larc.nasa.gov/tsab/cfdlarc/aiaa-dpw/Workshop4/workshop4.html. Accessed 5/18/2013.

[26] R. Voß and R. Thormann. Flutter computations for a generic reference aircraft adopting cfd and reduced order methods. In *Proceedings of 53rd AIAA/ASME/ASCE/AHS/ASC Structures, Structural Dynamics and Materials Conference, 23–26 April 2012, Honolulu, Hawaii*, 2012.

[27] R. Voß, L. Tichy, and R. Thormann. A ROM based flutter prediction process and its validation with a new reference model. In *IFASD 2011 - 15th International Forum on Aeroelasticity and Structural Dynamics, 27 - 30 June 2011, Paris, France*, 2011.